Hybrid Multiphase Fresnel Lenses on Silicon Wafers for Terahertz Frequencies

Surya Revanth Ayyagari, Simonas Indrišiūnas, and Irmantas Kašalynas, *Senior Member, IEEE*

***Abstract*—The hybrid multiphase Fresnel lenses (H-MPFLs) were developed on silicon wafer at the selected frequency of 585 GHz. For this reason, the design of a standard MPFL was modified thoroughly in various outer zone areas in order to reduce the complexity and manufacturing time of the diffractive optical elements by employing the direct laser ablation processes. The phase offset was found by precise control over the phase shift of incoming radiation in steps of $\pi/12$, revealing its optimal value to be of $+\pi/4$ independently on the hybridization order of the lens, the focusing gain of which was found to be up to 10 % higher than that achieved with a standard design MPFL. The numerical modeling data were confirmed by experiments demonstrating the effective THz beam focusing with H-MPFL samples to the diffraction-limited spot size. The proposed development procedure can be further modified by scaling the hybrid lens design to other frequencies with different zone numbers and/or by employing other materials suitable for THz photonics integration on-chip with the semiconductor devices.**

***Index Terms*—Direct laser ablation (DLA), hybrid multi-phase fresnel lenses (H-MPFLs), integrated photonics, phase control, terahertz (THz) frequencies.**

I. Introduction

As THE terahertz (THz) science and technologies progress rapidly in recent years, there is a request for optical components of high performance and less fabrication difficulty, which integration on-chip with the semiconductor devices would be less demanding [1], [2], [3]. A beam shaping with the diffractive optical elements (DOEs) grabs attention of the THz community because of their miniature size (order of wavelength), light weight, and compatibility with on-chip technologies with respect to reflective and refractive elements [4], [5], [6]. Depending on the dedicated function for example focusing, redirecting, and splitting of incoming radiation, a typical DOE may possess different structural forms based on the design rules of wave optics [7]. The multi-phase Fresnel lens (MPFL) is a successful example of DOE which defines the beam shape by describing the phase and amplitude distribution of incident wave at the focal plane. In general, MPFL may have different zone profiles like binary or multilevel step patterns which make a phase shift of incoming radiation resulting in constructive wave interference at a predefined distance along an optical axis. In a particular case, the thickness of material is adjusted to introduce the phase offsets strictly related to the value of the effective refractive index.

Different tools such as mechanical polishing, hot pressing, and 3D printing have been used for the development of the MPFLs as the discrete components of different low refractive index materials such as polymers, Teflon, polyamides, and paraffins which possess small optical losses in the sub-THz frequency range [8], [9], [10], [11]. All those materials and fabrication processes make bottleneck for the developments at higher THz frequencies and for the integration of MPFLs on-chip with other THz devices [2], [3]. Researchers moved to higher frequencies by making use of silicon (Si) with low absorption losses typical for many semiconductor crystals [12], [13]. Reactive ion etching [14] and photo-lithography [15] are the two most common methods used to manufacture Si-based MPFLs; however, they are tedious if several processing steps need to be modified [16]. A mask-less direct laser ablation (DLA) technology was proposed recently [17], [18] as a flexible tool for the development of MPFLs with different number of phase quantization levels (Q), which demonstrated good focusing performance in a wide frequency range from 0.6 up to 5 THz [19], [20]. Large Fresnel losses due to high refractive index of Si were proposed to compensate by fabrication of anti-reflection coatings within the same DLA process [21], [22], [23]. Notably that the diffraction efficiency of Si-based MPFLs with large Q value can reach almost 100% [19]. However, manufacturing of the MPFL with a large number of phase quantization levels is a challenging task because the complexity of step profile increases going toward the outer zones [20]. On the other hand, the design of lens with a high numerical aperture, defined as the ratio between the diameter and the focal distance, needs to be considered in the case of THz device manufacturing on-chip. Indeed, DLA processing of Si for THz technologies makes specific requirements for the surface smoothness and

Manuscript received 11 July 2022; revised 22 September 2022 and 29 December 2022; accepted 27 February 2023. Date of publication 11 April 2023; date of current version 3 May 2023. This work was supported in part by the EU TERAOPTICS project under Grant 956857 under the program H2020-EU.1.3.1. topic MSCA-ITN-2020 and in part by the "Hybrid plasmonic components for THz range (T-HP)" project under Grant DOTSUT-184 of the Research Council of Lithuania (Lietuvos Mokslo Taryba) funded by the European Regional Development Fund according to the Measure No. 01.2.2-LMT-K-718-03-0096. *(Corresponding author: Surya Revanth Ayyagari.)*

Surya Revanth Ayyagari is with the Terahertz Photonics Laboratory, Center for Physical Sciences and Technology (FTMC), LT-02300 Vilnius, Lithuania (e-mail: surya.revanth@ftmc.lt).

Simonas Indrišiūnas is with the Laser Microfabrication Laboratory, Center for Physical Sciences and Technology (FTMC), LT-02300 Vilnius, Lithuania (e-mail: simonas.indrisiunas@ftmc.lt).

Irmantas Kašalynas is with the Institute of Applied Electrodynamics and Telecommunications, Vilnius University, LT-10257 Vilnius, Lithuania, and also with the Terahertz Photonics Laboratory, Center for Physical Sciences and Technology (FTMC), LT-02300 Vilnius, Lithuania (e-mail: irmantas.kasalynas@ftmc.lt).

Color versions of one or more figures in this article are available at https://doi.org/10.1109/TTHZ.2023.3263638.

Digital Object Identifier 10.1109/TTHZ.2023.3263638

dimensions of the phase-delay-material used especially in the area of most outer zones [13], [24]. It is worth noting that only with the appearance of the DLA technology, many designs of DOEs become possible to realize crystal materials in the THz range [25], [26], [27]. Thus, new designs and optimization procedures of phase step profiles require a detailed investigation. The first attempts of simplification of the outermost zones of MPFLs by phase correction technique were made theoretically and experimentally by several groups [28], [29], [30]. However, to the best of our knowledge, the development of hybrid MPELs (H-MPFLs) with a similar or even better focusing performance than the standard design MPFL has not been reported.

In this work, the hybrid MPFLs were developed on high-resistivity float zone (HRFZ) Si wafer for radiation focusing at the selected frequency of 585 GHz. To realize the H-MPFL, we modified the design of standard MPFL with the phase quantization levels of eight ($Q = 8$), which has been previously demonstrated to be a good tradeoff between fabrication time, design complexity, and focusing performance [19], [20]. Simplification and successful optimization of outer zone parameters of standard MPFL lead to less demanding DLA fabrication process without deterioration of the focusing gain. The focal length, F, of 13 mm and the F-number of 1 were selected as initial parameters for the design. All MPFL samples were fabricated by the DLA technology, demonstrating very good THz beam focusing in agreement with numerical data. We believe that our findings are useful for further developments of laser-processed THz components and for THz photonics integration on-chip with semiconductor devices.

II. Numerical Modeling

A loss-free Si of 0.5 mm thickness (h) was selected for the development of the MPFL samples of different shapes and complexites. Namely, both-sides polished, (100) crystal orientation HRFZ-Si wafers with a resistivity of 100 kΩ cm and a refractive index of 3.45 were employed. The properties of HRFZ-Si after laser ablation have been investigated in the THz range elsewhere [24].

The standard MPFL was designed using the following equations [6]:

$$\mathrm{r_n} = \sqrt{\frac{2\lambda \mathrm{n}\left(\mathrm{F} + \frac{d}{2}\right)}{\mathrm{Q}} + \frac{\mathrm{n}^2\lambda^2}{\mathrm{Q}^2}} \tag{1}$$

here r_n is the outer radius of nth subzone (concentric ring), λ is the design wavelength, used value λ = 0.512 mm. The depth of single subzone, d, was described by equation

$$d = \frac{\lambda}{Q\left(\varepsilon - 1\right)}\left(1 + \frac{m}{8}\right) \tag{2}$$

here m is the integer number value which will be discussed later, ε is the refractive index of HRFZ-Si, the value of which was measured by THz time-domain spectroscopy to be approximately 3.45. To have a complete set of quantization levels, the total number of Fresnel zones (FZ) and concentric rings (n) in the design were fixed to integers of 3 and 3^*Q, respectively. Thus, the total diameter of the lenses was estimated to be about $D = 2^* r_{24} = 13.02$ mm.

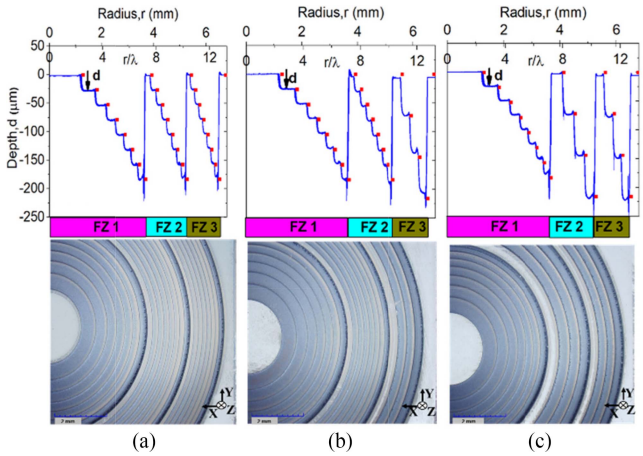

Fig. 1. Step profile across centrum line (top row) and microscope picture (bottom row) of the fabricated samples of (a) standard design MPFL with Q = 8 for all fresnel subzones (b) Optimized H-MPFL1 with $Q = 4$ and $m = +3$ at the most outer subzones area FZ3. (c) Optimized H-MPFL2 with $Q = 4$ and $m = +3$ at both FZ2 and FZ3 areas. The step profile for each sample was taken from the numerical design (Red dots) and measured by a "veeco dektak 150" profilometer (blue line).

In the case of standard MPFL, the parameter d was kept the same for all FZ. However, for lenses of hybrid design, the depth of subzones was varied with respect to the used value of Q. Fig. 1(a) demonstrates a step profile of standard design MPFL with $Q = 8$ from which the hybrid lens samples were developed with a smaller amount of phase quantization levels in the area of most outer zones [see Fig. 1(b) and (c)]. Each set of the FZ is indicated by different color bar at the bottom of Fig. 1(a) and (c). Two hybrid lens designs were obtained after modification Q from 8 to 4 value in one set of FZ 3 (FZ 3) and in two sets of zones 2, 3 (FZ 2, FZ 3) labeling these samples as H-MPFL 1 [see Fig. 1(b)] and H-MPFL 2 [see Fig. 1(c)], respectively. In addition, the H-MPFL 3 samples (not shown in Fig. 1) with a smaller amount of phase quantization levels, namely $Q = 2$ at zone 3 (*FZ 3*), were also considered.

A finite difference time domain method using CST software was used to analyze and optimize the focusing performance of the samples. The focusing gain was defined as the squared ratio between the field amplitude with (E_{MPFL}) and without (E_0) lens under research. The simulations were performed by choosing perfectly matched layer boundary conditions in order to absorb the transmitted and reflected waves from the structure. Symmetric conditions were enforced in X (perfect electric) and Y directions (perfect magnetic) to reduce simulation time and working memory requirements. The calculations were performed assuming the steady-state energy criterion using a multifrequency plane wave with a field amplitude of 1 V/m irradiation onto the sample. The intensity distribution along the optical axis and at the focal plane was calculated and analyzed. Fig. 2 shows simulated focusing gain characteristics obtained for the selected samples. Calculated beam profiles normalized to input radiation for the standard MPFL are shown in Fig. 2 by

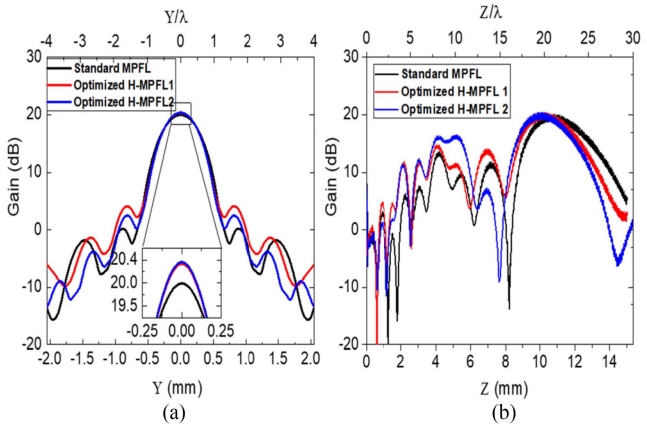

Fig. 2. Simulated focusing gain characteristics at (a) focal plane and (b) along optical axis for the standard MPFL sample and two optimized H-MPFL1 and H-MPFL2 samples with the same parameters as in Fig. 1. The results are shown in semi-log scale, where dB = 10 log (Gain). Inset shows the gain characteristics of the same samples in linear scale in the zoomed area. Note, bottom axis is in millimeters, whereas top is normalized to the design wavelength λ.

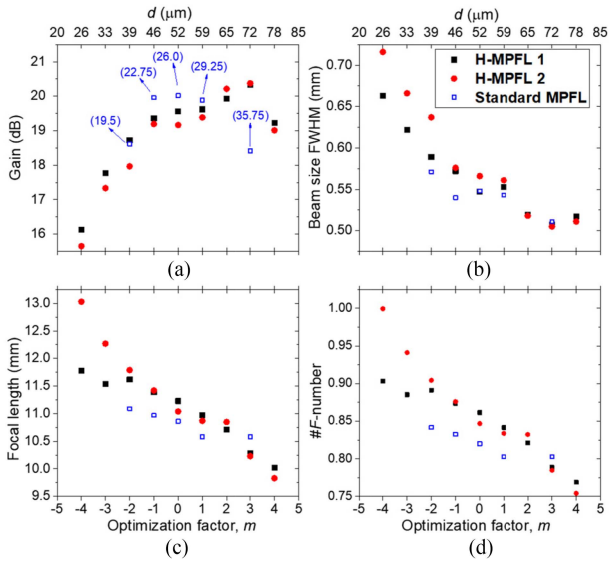

Fig. 3. (a) Simulated focusing gain, (b) FWHM, (c) focal distance, and (d) #*F*-number of the standard MPFL, H-MPFL1, and H-MPFL2 samples with different value of the optimization factor (*m*), bottom *x*-axis, and resulting depth of subzones, *d*, top *x*-axis. Inset: Numbers in brackets, which are shown only in (a), indicate actual *d* value in micrometers of subzones with respect to the optimization factor for the standard MPFL samples.

black solid lines. The gain value without taking into account a reflection loss was found to be about 20 dB (about 100 times) which is in agreement with data obtained from the analytical performance description of the MPFL used [6], [20].

The optimization of phase profile in the selected outer FZ areas of the H-MPFL samples was performed by using a discrete step size of one-eighth $(m/8)$ of the depth initial value at the subzone area in (2) until the lens reached a maximum value of the focusing gain. For this reason, an integer m value was varied in the range from -4 to $+4$, which corresponds to a phase change of $\pi/12$ for the selected wavelength. The optimization results in terms of the focusing gain, beam size, focal distance, and #*F*-number of the MPFL samples with hybrid phase profile with respect to the standard MPFL as a function of optimization factor (m) are shown in Fig. 3.

The change of the depth in subzones area modifies the lens performance independently on the hybridization order of H-MPFL samples. Larger focusing gain was found by making the depth of subzones deeper for both hybrid design lenses than the actual subzone depth instead of making them shallower [see Fig. 3(a)]. The maximum gain was found when the optimization factor of $+3$ was added to the actual subzone depth of H-MPFL1 and H-MPFL2 samples, which corresponds to the phase increment of $\pi/4$. Moreover, we see the reduction in full-width half maximum (FWHM) of focused beam size at the same $m = +3$ [see Fig. 3(b)]. In addition, Fig. 3(c) and (d) demonstrate the modification of focal length and #*F*-number with very similar values as for the standard MPFL sample with $d = 26$ μm, when the optimization factor for H-MPFL samples is of about three-eighths of the actual subzone depth, i.e., $m = +3$. It is worth noting that the maximum gain for standard MPFL samples is achieved when $m = 0$, i.e., the performance of standard design diffractive lenses is optimal in terms of focusing gain, therefore, analytical (1) and (2) accurately describe geometry parameters of the MPFL.

TABLE I
SUMMARY OF THE MODELING RESULTS

Sample	Depth *d* at outer sub-zones (μm)	FWHM (mm)	Focusing Gain (dB)	#*F*-num.
Standard MPFL with Q=8 at all Fresnel zones (FZ=1,2,3.)				
Standard MPFL with *m*=0	26	0.548	20.0	0.82
Optimized H-MPFL with Q=4 at FZ=3; Q=8 at FZ=1, 2.				
H-MPFL1 with *m*=+3	72	0.507	20.3	0.78
Optimized H-MPFL with Q=4 at FZ=2,3; Q=8 at FZ=1.				
H-MPFL2 with *m*=+3	72	0.505	20.4	0.78
H-MPFL with Q=2 at FZ=3; Q=8 at FZ=1, 2.				
H-MPFL3 with *m*=0	104	0.616	17.5	0.89
Standard MPFL with Q= 8 at FZ = 1,2 without FZ=3.				
MPFL4 with *m*=0	26	0.590	17.6	0.96

Numerical optimization results are summarized in Table I. The H-MPFL1 and H-MPFL2 samples with factor $m = +3$ demonstrated maximum focusing gain and were treated as optimal design lenses, resulting in up to 10 % (+0.4 dB) higher gain in comparison to the standard MPFL [see also red and blue curves in Fig. 2(a) and (b)]. On other hand, the optimization of the H-MPFL3 samples was not carried out as their initial focusing gain was found to be small. Namely, the H-MPFL3 sample with $m = 0$ demonstrated the focusing gain to be up to 2 times smaller with respect to the reference sample and even smaller as compared to the MPFL4, which is a standard design MPFL with $Q = 8$ and $m = 0$ but with only two sets of FZ, namely *FZ* 1 and *FZ* 2. The increase in focusing gain for the optimized H-MPFL samples was due to constructive interference of the wavefront thanks to precise control over a phase shift of incoming radiation.

Further increase in the subzone depth, cases $m > +3$, resulted in the destructive interference and reduction of the focusing gain and FWHM values.

Moreover, from the results shown in Fig. 2(a), we clearly see a change in sidelobe level from 0.23 dB for standard MPFL to 4.05 dB for H-MPFL1 sample with an increase of absolute focusing gain at the central beam by up to 10% (+0.4 dB). Further modification of the hybrid lens design from H-MPFL1 to H-MPFL2 resulted in two times smaller sidelobe magnitude (2.48 dB) maintaining approximately the same focusing gain values at the central beam (see Table I).

III. Results Experimental Validation

Three samples in total, two of optimized design (H-MPFL1 and H-MPFL2) and one of standard MPFL design were fabricated for operation at the frequency of 585 GHz. The zone plates were patterned by an industrial-scale pulsed laser (Atlantic 60, EKSPLA UAB) with a pulse duration of 10 ps, operation wavelength of 1064 nm, scan speed of 856 mm/s (47 % spot overlap), 32 μm laser spot size diameter, 11.8 J/cm^2 laser irradiation fluence, hatch angle rotation of 45 deg after each scan, and etch depth of 0.2 μm per layer which allowed to maintain precise control over the profile shape of the MPFLs. Microscope pictures of the fabricated samples are shown in the bottom row of Fig. 1. The step profiles of each sample scanned with "Veeco Dektak 150" profilometer demonstrate a good fit to the design shape as shown from the center towards edge side in the top row of Fig. 1.

The outer subzones become increasingly narrower with growing distance from the center in a standard design MPFL. Therefore, a small spot size of the laser beam is needed to produce a large diameter lens and ensure sufficient fabrication resolution in the outer zone areas. Whereas the outer subzones in the hybrid lenses are wider but a bit deeper. Although the removed material volume in the standard design lens is smaller than that in the hybrid lenses, the feasibility to use a large diameter laser beam leads to a faster and less demanding fabrication process of those lenses. For example, if we consider the narrowest ring of the standard and hybrid design to be, respectively, 100 and 150 μm, then we increase proportionally the laser spot and 1.5 times faster fabricate hybrid lens of the optimized design.

Focusing performance of the samples was explored experimentally by using a THz continuous wave system operating at 585 GHz frequency. Setup is shown in Fig. 4. Briefly, it is composed of RF generator, amplifier, collimator (HDPE lens), reflecting off-axis parabolic mirror (Gold Mirror), microbolometric THz detector placed on scanning multiaxis translation stage, and lock-in amplifier for the signals readout and storage in the personal computer. The radiation generated by Schottky diode-based AMC (Amplification Multiplication Chain) was outcoupled via a horn antenna. The measurements were done by scanning with the THz detector placed on an automated 3D axis stage. This allowed us to evaluate the intensity distribution along the optical axis (Z-axis) and in the focal plane (X- and Y- directions) with respect to the sample.

The measurements revealed a Gaussian beam shape at the sample plane in experiments with FWHM = 14 mm (see inset in Fig. 4). Notably, the plane wave excitation was used in the numerical simulation resulting in overestimated gain values in comparison to the experimental data. We would assume that the aperture efficiency with the reflection losses in our experiment was within the range of 38%.

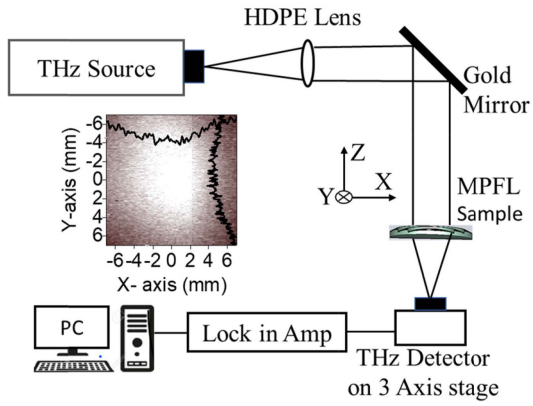

Fig. 4. Schematic representation of the experimental setup. Inset shows the Gaussian shape of the THz beam emitted from the THz source and measured at the position of MPFL sample. Noise of the THz signal recordings was approximately 0.1 mV, resulting in the noise level of focusing gain to be at about −10 dB.

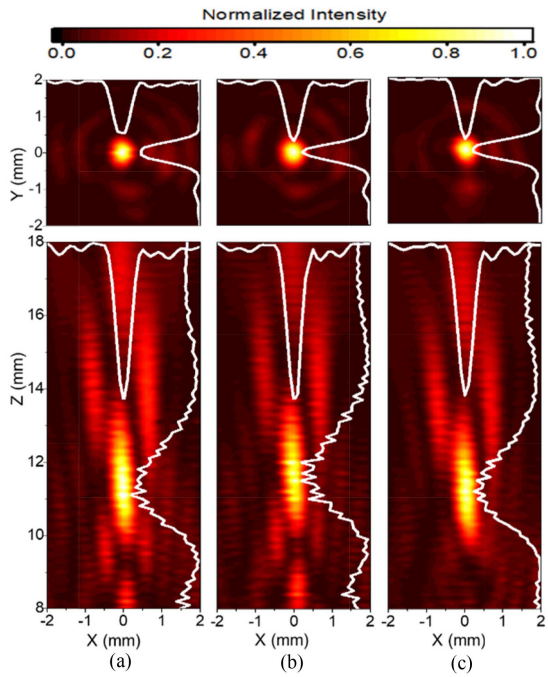

Fig. 5. THz beam intensity distribution measured at the focal plane (XY plane) and along the optical axis (XZ plane) with respective cross-section of focused beam for the fabricated (a) standard MPFL, (b) optimized H-MPFL 1, and (c) optimized H-MPFL 2 samples.

Experimental data of the THz beam focusing with different samples are shown in Fig. 5. The focal distance was found to be around 12 mm (z-direction) similar for all samples. It is clear that the beam is perfectly focused as an Airy disc seen in the focal plane as the side lobes around the central focal spot. The

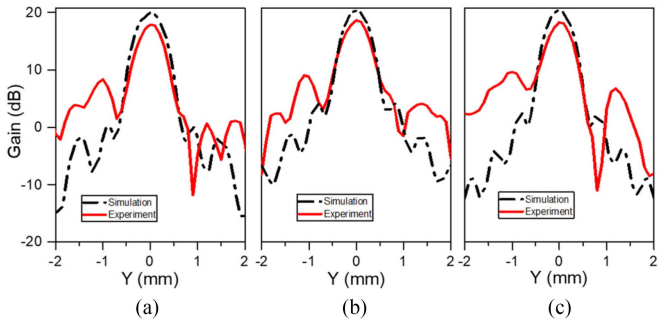

Fig. 6. Focusing gain in semi-log scale obtained experimentally (solid red lines) and numerically (dot-dashed black lines) at the focal plane for the (a) standard MPFL, (b) optimized H-MPFL 1, and (c) optimized H-MPFL 2 samples.

TABLE II
SUMMARY OF EXPERIMENTAL AND SIMULATION VALUES OF THE FWHM AND FOCUSING GAIN FOR THE FABRICATED MPFL SAMPLES

Sample	Simulation		Experiment	
	FWHM (mm)	Focusing Gain / dB	FWHM (mm)	Focusing Gain /dB
Standard MPFL	0.548	99.0/20.0	0.498	61.7/17.9
Optimized H-MPFL 1	0.507 (B=0.92)	108/20.3 (A=0.91)	0.527 (B=1.06)	73.5/18.7 (A=0.84)
Optimized H-MPFL 2	0.505 (B=0.92%)	109/20.4 (A=0.90)	0.498 (B=1.00)	68.2/18.3 (A=0.90)

increment in intensity was found in the experiment up to ∼10% (+0.4 dB) for the H-MPFL samples compared to the standard MPFL. It is worth noting that the magnitude of the intensity change was found the same as predicted by numerical modeling.

Fig. 6 demonstrates the focusing gain characteristics obtained experimentally and numerically for different lens samples. Both hybrid design lenses demonstrated the same #F-number and the focusing gain approx. Ten percent (0.4 dB) higher than values are achieved with the reference MPFL samples. Detailed comparison of experimental and modeling results for fabricated samples is done in Table II. The first columns of the simulation and experimental data show the focused beam FWHM measured along the Y-axis direction. From the beam width percentage ratio, B, of the beam size of hybrid, $\mathrm{FWHM_H}$, to the beam size of standard, $\mathrm{FWHM_S}$, design samples, i.e., $B = \mathrm{FWHM_H} / \mathrm{FWHM_S}$, we conclude that the focused beamwidth of optimized H-MPFL samples is narrowed by up to 8% compared to the standard MPFL in simulation, whereas from the experimental data, a similar change of FWHM values was found. The comparison of focusing gain was evaluated as the attenuated gain, A, indicating the ratio between the focusing gain of standard, G_S, and hybrid, G_H, design MPFL samples, i.e., $A = G_S, / G_H$. Here $A < 1$ indicates the focusing gain of the hybrid design lens to be higher in comparison to standard design MPFL. By comparing the A values, we clearly see that the optimized H-MPFL samples demonstrated slightly better focusing performance both in theory and in experiment. It is worth to mention that by measuring the ratio between intensities at the focused beam center and the side of first-order lobe, the diffraction efficiency was estimated to be about 93 % (98 %) in the experiment (in modeling), the value of which was in agreement with the analytical description of the MPFL [6], [20].

We can also see from Table II a noticeable change in the focusing gain of about 7 % and beam size of about 6 % in the experiment values for optimized H-MPFL 2 compared to optimized H-MPFL 1 samples. Such differences were in the range of experimental errors as the simulation data demonstrated a considerably smaller difference between respective parameters of the optimized hybrid samples being only about 0.9% and 0.3%, respectively (see also Figs. 2 and 3).

Thus, obtained results validate a successful optimization process of the hybrid lenses with reduced complexity of phase profile. The H-MPFL samples demonstrated in the experiment slightly better focusing performance as those of standard design MPFL samples. The increment in the focusing gain of hybrid lenses was attributed to smaller shadowing effects and more efficient constructive interference of the spherical wavefront because of precise control over the phase shift of incoming radiation at the outer FZ by making them deeper [31], [32], [33]. Achieved overall focusing gain, which was not a concern of this research work, from the optimized H-MPFL samples was up to 18.7 dB (20.4 dB) in the experiment (numerical modeling), can be further increased with a larger amount of the FZ [6], [20].

IV. CONCLUSION

To conclude, we have developed for selected frequency the H-MPFLs with two times smaller number of steps in the phase profile at most outer FZ areas. Optimal phase offset was found to be of $+\pi/4$ independently on the hybridization order of the H-MPFL samples, the focusing gain of which was found to be up to 10% higher in comparison to a standard design MPFL. Thus, we proposed a new approach for the development of much simpler and less complex DOEs which can be scaled to other frequencies and integrated on semiconductor chips with THz detectors and emitters.

REFERENCES

[1] J. Engelberg and U. Levy, "Achromatic flat lens performance limits," *Optica*, vol. 8, no. 6, pp. 834–845, Jun. 2021, doi: 10.1364/OPTICA.422843.
[2] S. Al-Daffaie, A. J. Jumaah, V. L. Rubio, and T. Kusserow, "Design and implementation of a terahertz lens-antenna for a photonic integrated circuits based THz systems," *Sci. Rep.*, vol. 12, no. 1, Dec. 2022, Art. no. 1476, doi: 10.1038/s41598-022-05338-0.
[3] L. Minkevičius et al., "On-chip integration of laser-ablated zone plates for detection enhancement of InGaAs bow-tie terahertz detectors," *Electron. Lett.*, vol. 50, no. 19, pp. 1367–1369, 2014, doi: 10.1049/el.2014.1893.
[4] D. Headland, Y. Monnai, D. Abbott, C. Fumeaux, and W. Withayachumnankul, "Tutorial: Terahertz beamforming, from concepts to realizations," *Amer. President Lines Photon.*, vol. 3, no. 5, May 2018, Art. no. 051101, doi: 10.1063/1.5011063.
[5] A. Siemion, "The magic of optics—An overview of recent advanced terahertz diffractive optical elements," *Sensors (Switzerland)*, vol. 21, no. 1, pp. 1–22, Jan. 2021, doi: 10.3390/s21010100.
[6] H. D. Hristov, *Fresnel Zones in Wireless Links, Zone Plate Lenses, and Antennas*. Norwood, MA, USA: Artech House, 2000.
[7] W. T. Chen and F. Capasso, "Will flat optics appear in everyday life anytime soon?," *Appl. Phys. Lett.*, vol. 118, no. 10, Mar. 2021, Art. no. 100503, doi: 10.1063/5.0039885.
[8] V. M. Vedernikov et al., "Diffractive elements for a free electron laser," *Optoelectron. Instrum. Data Process.*, vol. 46, no. 4, pp. 365–375, Aug. 2010, doi: 10.3103/s8756699010040102.

[9] W. D. Furlan et al., "3D printed diffractive terahertz lenses," *Opt. Lett.*, vol. 41, no. 8, Apr. 2016, Art. no. 1748, doi: 10.1364/ol.41.001748.
[10] A. Siemion et al., "Paraffin diffractive lens for subterahertz range—Simple and cost efficient solution," *IEEE Trans. Terahertz Sci. Technol.*, vol. 11, no. 4, pp. 396–401, Jul. 2021, doi: 10.1109/TTHZ.2021.3063809.
[11] V. B. Yurchenko, M. Ciydem, M. Gradziel, J. A. Murphy, and A. Altintas, "Double-sided split-step MM-wave Fresnel lenses: Design, fabrication and focal field measurements," *J. Eur. Opt. Soc. Rapid Pub.*, vol. 9, Feb. 2014, Art. no. 14007, doi: 10.2971/jeos.2014.14007.
[12] T. V. Kononenko et al., "Silicon kinoform cylindrical lens with low surface roughness for high-power terahertz radiation," *Opt. Laser Technol.*, vol. 123, Mar. 2020, Art. no. 105953, doi: 10.1016/j.optlastec.2019.105953.
[13] S. Indrisiunas et al., "Laser-processed diffractive optics for terahertz waves," in *Proc. Int. Conf. Adv. Optoelectron. Lasers*, 2019, pp. 1–4, doi: 10.1109/CAOL46282.2019.9019480.
[14] A. N. Agafonov et al., "Silicon diffractive optical elements for high-power monochromatic terahertz radiation," *Optoelectron. Instrum. Data Process.*, vol. 49, no. 2, pp. 189–195, Mar. 2013, doi: 10.3103/s875669901302012x.
[15] D. K. Woo, K. Hane, C. B. Lee, and S. K. Lee, "Fabrication of a multi-level lens using independent-exposure lithography and FAB plasma etching," in *Proc. IEEE/LEOS Int. Conf. Opt. Micro-Electromech. Syst. Nanophoton.*, 2007, pp. 151–152, doi: 10.1109/OMEMS.2007.4373885.
[16] P. Pal and K. Sato, "A comprehensive review on convex and concave corners in silicon bulk micromachining based on anisotropic wet chemical etching," *Micro Nano Syst. Lett.*, vol. 3, no. 1, Dec. 2015, Art. no. 6, doi: 10.1186/s40486-015-0012-4.
[17] B. Voisiat et al., "Laser processing for precise fabrication of the THz optics," in *Proc. Int. Soc. Opt. Eng.—Int. Soc. Opt. Eng.*, 2017, vol. 10091, pp. 66–75, doi: 10.1117/12.2253634.
[18] G. Raciukaitis, "Ultra-short pulse lasers for microfabrication: A review," *IEEE J. Sel. Topics Quantum Electron.*, vol. 27, no. 6, Nov./Dec. 2021, Art. no. 1100112, doi: 10.1109/JSTQE.2021.3097009.
[19] L. Minkevičius et al., "Terahertz multilevel phase Fresnel lenses fabricated by laser patterning of silicon," *Opt. Lett.*, vol. 42, no. 10, pp. 1875–1878, 2017, doi: 10.1364/OL.42.001875.
[20] S. Indrišiūnas et al., "Laser-processed diffractive lenses for the frequency range of 47 THz," *Opt. Lett.*, vol. 44, no. 5, Mar. 2019, Art. no. 1210, doi: 10.1364/OL.44.001210.
[21] J. A. Dobrowolski and F. Ho, "High performance step-down AR coatings for high refractive-index IR materials," *Appl. Opt.*, vol. 21, no. 2, pp. 288–292, Jan. 1982, doi: 10.1364/AO.21.000288.
[22] M. Tamosiunaite et al., "Focusing of terahertz radiation with laser-ablated antireflective structures," *IEEE Trans. Terahertz Sci. Technol.*, vol. 8, no. 5, pp. 541–548, Sep. 2018, doi: 10.1109/TTHZ.2018.2859619.
[23] H. Sakurai et al., "Terahertz broadband anti-reflection moth-eye structures fabricated by femtosecond laser processing," *Opt. Soc. Amer. Continuum*, vol. 2, no. 9, Sep. 2019, Art. no. 2764, doi: 10.1364/OSAC.2.002764.
[24] S. Indrisiunas et al., "Laser-ablated silicon in the frequency range from 0.1 to 4.7 THz," *IEEE Trans. Terahertz Sci. Technol.*, vol. 9, no. 6, pp. 581–586, Nov. 2019, doi: 10.1109/TTHZ.2019.2939554.
[25] Y.-H. Liu, K.-K. Kuo, C.-W. Cheng, and A.-C. Lee, "Femtosecond laser two-beam interference applied to 4H-SiC surface hierarchical micro-nano structure fabrication," *Opt. Laser Technol.*, vol. 151, Jul. 2022, Art. no. 108081, doi: 10.1016/j.optlastec.2022.108081.
[26] R. Takaku et al., "Broadband, millimeter-wave anti-reflective structures on sapphire ablated with femto-second laser," *J. Appl. Phys.*, vol. 128, no. 22, Dec. 2020, Art. no. 225302, doi: 10.1063/5.0022765.
[27] R. Takaku et al., "Large diameter millimeter-wave low-pass filter made of alumina with laser ablated anti-reflection coating," *Opt. Exp.*, vol. 29, no. 25, Dec. 2021, Art. no. 41745, doi: 10.1364/OE.444848.
[28] Y. J. Guo and S. K. Barton, "On the subzone phase correction of Fresnel zone plate antennas," *Microw. Opt. Technol. Lett.*, vol. 6, no. 15, pp. 840–843, Dec. 1993, doi: 10.1002/mop.4650061505.
[29] B. Kuhlow, M. Ferstl, E. Pawlowski, G. Przyrembel, and P. C. M. Galloway, "Multilevel Fresnel zone lenses capable of being fabricated with only one binary mask," in *Proc. Curr. Develop. Opt. Des. Opt. Eng.*, 1994, vol. 2263, pp. 102–113, doi: 10.1117/12.187991.
[30] E. Antonov, M. Fu, V. Petrov, D. Manko, and K. Rong, "Structure of microprismatic Fresnel lenses for creating uniform focal images," *Opt. Exp.*, vol. 29, no. 24, Nov. 2021, Art. no. 38958, doi: 10.1364/OE.438590.
[31] D. W. Prather, D. Pustai, and S. Shi, "Performance of multilevel diffractive lenses as a function of f-number," *Appl. Opt.*, vol. 40, no. 2, pp. 207–210, Jan. 2001, doi: 10.1364/AO.40.000207.
[32] J. Suszek et al., "Evaluation of the shadow effect in terahertz kinoform gratings," *Opt. Lett.*, vol. 38, no. 9, May 2013, Art. no. 1464, doi: 10.1364/ol.38.001464.
[33] M. Rachon et al., "Enhanced sub-wavelength focusing by double-sided lens with phase correction in THz range," *J. Infrared, Millim., Terahertz Waves*, vol. 41, no. 6, pp. 685–696, Jun. 2020, doi: 10.1007/s10762-020-00696-0.

Surya Revanth Ayyagari received the Bachelor's degree in mechanical engineering (B.tech) from the Koneru Lakshmaiah University (KLU), Guntur, India, in 2015, and the Master's degree in optics and photonics (MSc in KSOP) from the Karlsruhe Institute of Technology (KIT), Karlsruhe, Germany, in 2020.

In 2018–2019, he worked as a Research Assistant with Tampere University, Tampere, Finland on "Nanophotonics." He is currently a Doctoral student with the Center for Physical Sciences and Technology (FTMC), Vilnius, Lithuania, being involved in the project TERAOPTICS of Marie Skłodowska-Curie Innovative Training Network (H2020-MSCA-ITN-2020) as an Early Stage Researcher (ESR), since January 2021. He is working towards Ph.D. thesis on "Diffractive optics integration with THz detectors and emitters."

Simonas Indrišiūnas received the Ph.D. degree in materials science from the Vilnius University, Vilnius, Lithuania, in 2018.

He is currently working with the Center for Physical Sciences and Technology, Department of Laser Technologies, Vilnius, Lithuania. His research interests include laser microfabrication technologies, in particular, parallel laser processing (laser interference patterning) for surface wetting control and other applications and fabrication of THz optical components using laser micromachining.

Irmantas Kašalynas (Senior Member IEEE) received the Ph.D. degrees in physics from the Vilnius University, Vilnius, Lithuania, in 2004.

In 2005, he was a Postdoc with the Terahertz Imaging Group, Faculty of Applied Science, Delft University of Technology, Delft, The Netherlands, working on THz detectors arrays and THz quantum cascade lasers. After Postdoc, he joined a THz Atelier group in Vilnius, Lithuania. In 2012/2013 and 2016/2017, he was on an internship with the Institute of High Pressure Physics, Warsaw, Poland, working on GaN-heterostructures and devices. Since 2013, he has been the Head of Terahertz Photonics Laboratory, Center for Physical Sciences and Technology, Vilnius, Lithuania, where he has attracted agency fundings exceeding 2 M€. He was a Co-Founder of Lithuanian-Slovenian Joint Stock start-up company LuviTERA UAB. Since 2021, he serves as a Professor of physics with Vilnius University. His research interests include THz device physics, THz optics and plasmonics, spectroscopic THz imaging, and application of THz waves.